Multiscale design of nanoengineered matrices for lead-free piezocomposites: Improved performance via controlling auxeticity and anisotropy

Jagdish A. Krishnaswamy [a,*], Federico C. Buroni [b], Roderick Melnik [a,c], Luis Rodriguez-Tembleque [c], Andres Saez [c]

[a] MS2Discovery Interdisciplinary Research Institute, Wilfrid Laurier University, 75 University Ave W, Waterloo, Ontario N2L 3C5, Canada
[b] Department of Mechanical Engineering and Manufacturing, Universidad de Sevilla, Camino de los Descubrimientos s/n, Seville E-41092, Spain
[c] Department of Continuum Mechanics and Structural Analysis, Universidad de Sevilla, Camino de los Descubrimientos s/n, Seville E-41092, Spain

ARTICLE INFO

ABSTRACT

Multiscale material design has made it possible to control the properties of a material through introducing structures at multiple length scales. This structuring brings about unusual material behaviour that is not seen in a continuum material. Here we introduce a multiscale design for the matrix components of a lead-free piezo-composite. This combines a microscale stiff polymeric structure embedded within a softer matrix to form a composite matrix. By controlling the microscale features of the embedded structure, we tune the mechanical behaviour of the matrix by rendering it either nonauxetic (hexagonal structure) or auxetic (inverted hexagonal structure). Further, the mechanical and electrical properties of the matrix are controlled at the nanoscale by addition of carbon nanotubes within the embedded polymeric structure. By engineering the matrix at the nano and the microscale, we firstly demonstrate that the auxetic matrix can result in three orders of magnitude higher piezoelectric response by amplifying the strains within the piezoelectric inclusions. We further demonstrate that by using the matrix with the nonauxetic embedded structure, it is possible to design piezoelectric composites with pronounced anisotropy in their longitudinal and transverse responses. This is an important requirement for designing materials with directional sensing ability. Our findings show that the multiscale material design proposed here has important implications for both energy harvesting and directional sensing. Further, the approach taken here yields considerable performance improvements while using limited quantities of nanomaterial. The multiscale matrix design is scalable and amenable to fabrication through emerging methods such as additive manufacturing.

1. Introduction

Lead-free piezocomposites are promising environmentally friendly alternatives to lead-based materials for interconversion between mechanical and electrical energies [1]. However, the gap in the performance between these classes of materials, with lead-free materials having a large scope for improvement, presents unique challenges in material design [1]. From the perspective of sensing and energy harvesting, this lag in the performance is due to multiple bottlenecks in the material behaviour. The first involves weak coupling of applied strains to the piezoelectric inclusions through the soft matrix material which absorbs most of the strain [2]. This happens because of large contrast in the elastic properties between the stiff piezoelectric crystalline inclusions and the significantly softer surrounding matrix. A second bottleneck involves the impeded flow of the generated flux

from the inclusions through the composite, resulting in its loss and a reduced sensitivity or harvesting capability. This arises again because of the large contrast in the permittivity of the inclusions (ε_r $10^2 - 10^3$ [3]) and the matrix (ε_r $10^0 - 10^1$ [4,5]). In the past, these performance barriers were addressed through designs with nano-modified matrices which were stiffer and simultaneously possessed higher permittivity. This was achievable through the controlled addition of nanomaterials such as carbon nanotubes, graphene, and so on, which possessed excellent mechanical and electrical properties that allowed simultaneous addressing of multiple design issues [2,6–10].

The application of classical approaches, however, is connected with some challenges. Firstly, these approaches involve using expensive nanomaterials which are distributed throughout the matrix of the composite. Secondly, the addition of such materials leads to significant composite stiffening [11–13] and the resulting composite might not

be soft enough for many applications involving implantable, wearable, and flexible devices and circuits. Therefore, it is important to conceive novel approaches that reduce the usage of nanomaterials. A second challenge in the area of sensing is the need to develop piezoelectric materials with the ability to selectively sense particular strain components [14,15], which cannot be addressed by the conventional ceramic materials due to their transverse isotropy. Therefore, geometrical design of composites for anisotropic piezoelectric response is an aspect of pressing importance in the area of sensing. Conventional composite design using nanomodification throughout the matrix is not suitable for this requirement and structured materials which can be manufactured by processes such as 3D printing [14,16,17] are inevitable.

The above challenges entail identifying new methods of enhancing the mechanical and electrical performance of composites. Along these lines, it was recently demonstrated that an auxetic matrix based entirely on structured polymeric materials can lead to dramatic improvements in the mechanical coupling within the composite [18]. This was based on earlier reports which investigated the role of auxetic structures and components in improving the mechanical coupling in piezoelectric materials and composites [19–21]. We use these results as a starting point to introduce a new multiscale matrix design.

Multiscale design implies the introduction of structural features at more than one length scale in a material [22]. Such design has the potential to impart unusual properties to materials which would not have been possible conventionally. This possibility arises due to the coexistence of multiple enhancement phenomena at different length scales. Here we combine microscale and nanoscale processes by conceiving a multiscale design for the matrix of a lead-free piezocomposite. The multiscale matrix is designed by embedding a relatively stiffer polymeric microstructured network structure within a softer matrix. The embedded microstructure is further subject to addition of carbon nanotubes, which allows tuning its mechanical and electrical properties. By tuning the microstructure, we design two matrix structures with similar nanofiller loadings but with nonauxetic and auxetic characteristics. A motivation for considering auxetic architectures is a recent demonstration of a piezoelectric enhancement mechanism based on auxetic matrices [18] and also the additional advantages of auxetic structures such as better stiffness [23], excellent tunability in mechanical properties such as Young's moduli of composites [24,25], and so on. Further, the microstructures are anisotropic and thus the resulting matrices have anisotropy in their elastic and dielectric properties. We will show that the auxetic and nonauxetic matrices with optimal nanoengineering of their electrical and mechanical properties, coupled with the polycrystalline nature of the BaTiO$_3$ piezoelectric inclusions, can lead to multiple design advantages. First, the auxetic design leads to an isotropic increase in the sensitivity to all strain components. This happens through improved coupling of applied mechanical stimuli by amplifying the strain within the inclusions. This is an important aspect in the design of composites optimized for energy harvesting. Further, the nonauxetic structure with optimal CNT loading within the microscale network and optimal BaTiO$_3$ polycrystallinity, can lead to significant anisotropy between the transverse and longitudinal piezoelectric response. This way, we will demonstrate that by controlling structures at multiple length scales – the microscale matrix structure and the nanoscale addition of carbon nanotubes – in addition to controlling the polycrystalline microstructure of the piezoelectric inclusions, it is possible to design piezocomposites with superior performance characteristics, specific to the needs of both energy harvesting and directional sensing applications.

In the following sections, we first provide a brief introduction to the theoretical aspects of piezocomposite design including the mathematical framework, material properties, and the boundary conditions that are used in the investigation. This will be followed by the results, discussion, and summary of the findings.

2. Electro-elastic model and boundary conditions

The development of the model proceeds in the following sequence: first, the effective electro-elastic coefficients of the matrix possessing the multiscale design are evaluated. Following this, the piezoelectric composite is modelled as a distribution of randomly shaped and positioned BaTiO$_3$ inclusions within a matrix that is modelled using the homogenized properties obtained from the first computational step. The effective elastic and piezoelectric coefficients of the piezocomposite are then computed as a function of the nano-filler within the microscale structures in the matrix. The following sections provide the details of the composite architectures investigated (Section 2.1), the electro-elastic model and the boundary conditions relevant to the study (Section 2.2), and the material properties (Section 2.3).

2.1. Composite architecture

We discuss two composite geometries we will model here. The first stage of the computation involves the evaluation of the effective elastic and dielectric properties of composite matrices, which will be used as homogenized matrix properties in the second stage of the computation which models the piezoelectric composites.

A representative volume element (RVE) consisting of a matrix and piezoelectric inclusions, which we investigate here is shown in Fig. 1 (a), with this particular example showing 9 randomly shaped and positioned BaTiO$_3$ inclusions. Fig. 1(b), further shows the representative volume elements of the matrix which has a microstructure which is composed of a network of either hexagonal and inverted hexagonal cells. Both the matrix architectures, as further shown in Fig. 1(c) comprise of a base matrix, PEGDA, which is a soft material within which a microstructured network structure made of a stiffer polymer (Epoxy LY5052) is embedded. The volume fraction of the microstructure is the same in the both matrices. However, the matrix composed of hexagonal repeating units has positive Poisson's ratio and that composed of inverted hexagonal repeating units has negative Poisson's ratio in the $x_1 - x_3$ plane. The important geometric parameters of the embedded epoxy structure are shown in Fig. 1(b). Table 1 further summarizes the values used for these parameters. These values are chosen from experimental data in the literature followed by scaling down the size of the structures [26]. Such composite structures could be fabricated using additive manufacturing [26] of the embedded structure followed by infusion of the polymeric material modified by addition of the piezoelectric material. Further, the epoxy is also modified through the addition of multiwalled carbon nanotubes ((15,15) MWCNTs), which will modify both the elastic and dielectric properties of the embedded material. In particular, the embedded epoxy becomes stiffer and its permittivity increases following a percolative relation $\varepsilon^{eff} = \varepsilon \left(\frac{f_p}{f_p - f_{CNT}} \right)^p$ [27,28]. Here, ε is the permittivity of the pristine material, f_p is the percolation threshold, p is the critical exponent, and f_{CNT} is the volume fraction of the MWCNTs in the epoxy. As $f_{CNT} \rightarrow f_p$, the effective permittivity of the composite material escalates to very high values. The effective elastic properties of the CNT-modified epoxy are obtained through the approaches highlighted in [29] and the results are provided in Appendix A1, along with the effective dielectric properties. The two matrix microstructures shown in Fig. 1(b) are well-studied architectures which can serve as representative examples of non-auxetic and auxetic architectures both comprising the same volume of the embedded epoxy and nanomaterial. We obtain the effective elastic and dielectric properties of these matrices in the first step of the computation by using the RVEs shown in Fig. 1(b) for the auxetic and nonauxetic architectures.

Further, we use the effective properties obtained from the first step to model the piezoelectric composites which consist of the lead-free polycrystalline BaTiO$_3$ inclusions embedded in the matrices. The inclusions are randomly shaped and are around 50 μm in size, which is
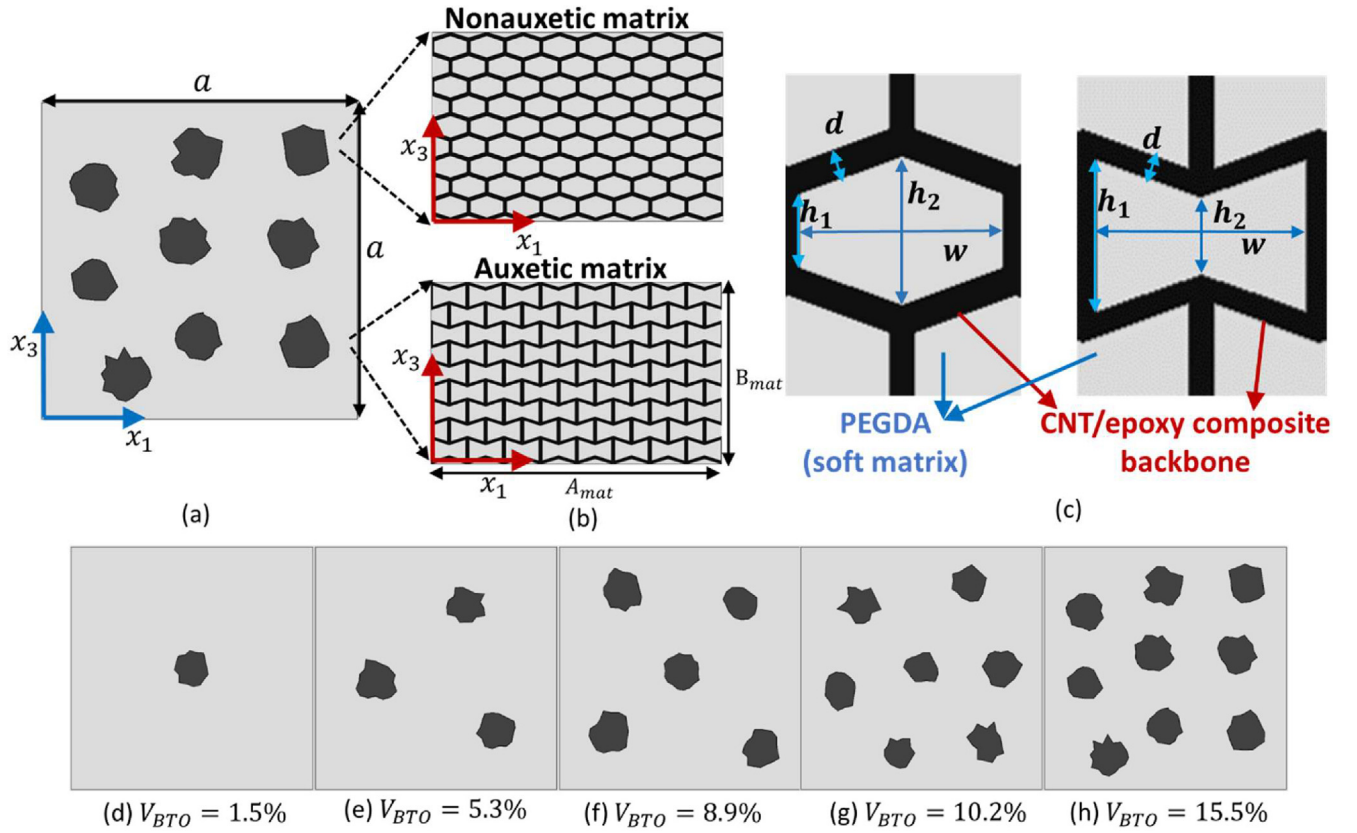
Fig. 1. (a) An exemplary RVE of a piezocomposite architecture investigated here showing the two matrix architectures – nonauxetic and auxetic – considered for comparison, (b) the hexagonal and inverted hexagonal repeating units embedded in the soft matrix base material (PEGDA) with the important geometric design parameters, (c)-(g) RVEs of the piezocomposites with progressively increasing inclusion concentration V_{BTO}.

Table 1
Geometric parameters of the matrix microstructure (refer to Fig. 1(c)).

Geometric parameter	Value (μm)	
	Nonauxetic architecture	Auxetic Architecture
w	9	9
h_1	3	6
h_2	6	3
d	1	1

much larger than the feature sizes in the microstructured matrices. This allows the use of homogenized properties for the matrix. The RVEs for the piezocomposite are shown in Fig. 1(d)-(h), with increasing BaTiO$_3$ inclusion concentrations V_{BTO}. As already mentioned, we assume effective homogenized properties for the matrix here, which are obtained from the first stage of computations.

2.2. Electro-elastic model

Here, we briefly provide the details of the constitutive and governing models that describe the electro-elastic behaviour and coupling. The electro-elastic fields – stress, strain, electric flux and electric fields are related through the following coupled equations of the piezoelectric model [30–33]:

$$\sigma_{ij} = c_{ijkl}\varepsilon_{kl} - e_{kij}E_k, \tag{1a}$$

$$D_i = \varepsilon_{ij}E_j + e_{ijk}\varepsilon_{jk} \tag{1b}$$

where σ_{ij} and ε_{kl} are the stress and strain tensor components and E_i and D_i are the electric field and flux density components. The coefficients c_{ijkl}, ε_{ij}, are e_{ijk} the components of the elastic, dielectric (or permittivity), and the piezoelectric tensors, respectively, of the material in question.

Eqs. (1a) and (1b) are further subject to the following governing equations for the force balance and electric flux balance:

$$\sigma_{ij,j} - F_i = 0, \tag{2a}$$

$$D_{i,i} = 0 \tag{2b}$$

where F_i refers to the components of the body force, which we assume to be zero in this study.

As seen from Fig. 1, these equations will be solved on two kinds of architectures – first, the RVE describing the multiscale matrix (Fig. 1 (b)), and second, the piezoelectric composite (Fig. 1(d)-(h)). In general, the RVE under examination is rectangular and has sides A_m and B_m, as shown in Fig. 2(a). If the RVE in question is that of the matrix (Fig. 1(a)), then we have $A_m = A_{mat}, B_m = B_{mat}$. If, on the other hand, the RVE is that of a piezocomposite architecture (Fig. 1(d)-(h)), then we have $A_m = B_m = a$. To extract the effective properties of these composite architectures which include the RVEs are subject to various boundary conditions BC1-BC5, as shown in Fig. 2(b)-(f). These are specialized boundary conditions used to obtain homogenized effective properties from RVEs [31,32].

Table 2, further, summarizes the calculation of the effective properties of the composite using these boundary conditions. The constitutive equations (Equations (1a)-(1b)) subject to the governing equations (Equation (2a)-(2b)) were solved by finite element analysis.

2.3. Material properties

As we have seen in Section 2.1 on the composite architecture, we study two levels of composite designs. At the first level, we have a
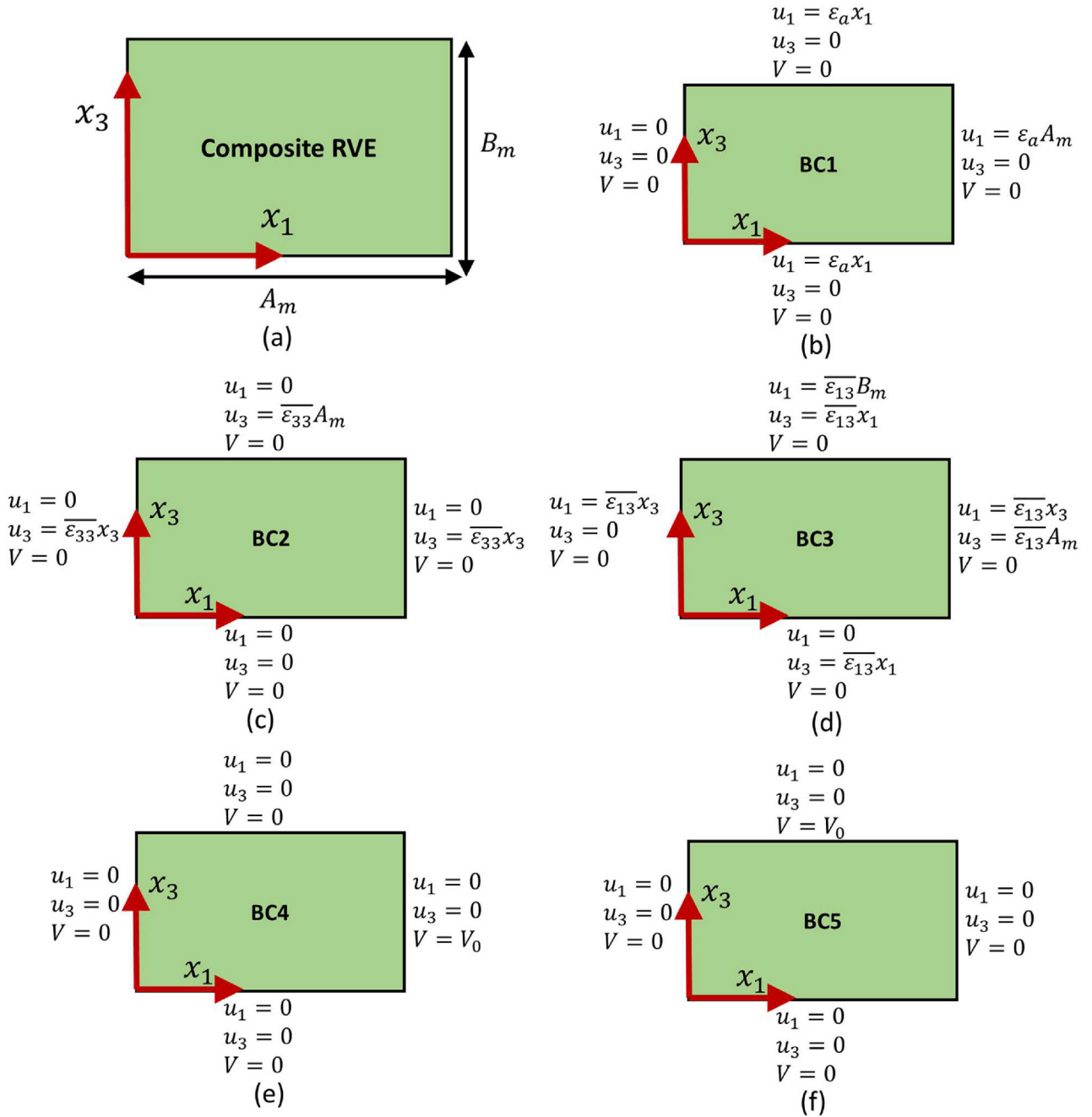
Fig. 2. (a) shows a generalized schematic of a rectangular RVE investigated here, which can correspond to either the RVE of the matrix (Fig. 1(b)) or that of the piezocomposite (Fig. 1(d)-(h)), (b)-(e) show the boundary conditions BC1-BC5 which are used to obtain the effective electro-elastic coefficients of the composite as highlighted in Table 2.

Table 2
Boundary conditions and the calculation of effective electro-elastic composite coefficients.

Boundary condition	Effective property calculation
BC1	$c_{11}^{eff} = \frac{1}{A_m B_m} \frac{\langle \sigma_{11} \rangle}{\varepsilon_{11}} c_{13}^{eff} = \frac{1}{A_m B_m} \frac{\langle \sigma_{33} \rangle}{\varepsilon_{11}} e_{31}^{eff} = \frac{1}{A_m B_m} \frac{\langle D_3 \rangle}{\varepsilon_{11}}$
BC2	$c_{11}^{eff} = \frac{1}{A_m B_m} \frac{\langle \sigma_{11} \rangle}{\varepsilon_{33}} c_{13}^{eff} = \frac{1}{A_m B_m} \frac{\langle \sigma_{33} \rangle}{\varepsilon_{33}} e_{33}^{eff} = \frac{1}{A_m B_m} \frac{\langle D_3 \rangle}{\varepsilon_{33}}$
BC3	$c_{44}^{eff} = \frac{1}{A_m B_m} \frac{\langle \sigma_{13} \rangle}{2\varepsilon_{13}} e_{15}^{eff} = \frac{1}{A_m B_m} \frac{\langle D_1 \rangle}{\varepsilon_{13}}$
BC4	$\varepsilon_{11}^{eff} = \frac{\langle D_1 \rangle}{\left(-\frac{V_0}{A_m}\right)\varepsilon_0}$
BC5	$\varepsilon_{33}^{eff} = \frac{\langle D_3 \rangle}{\left(-\frac{V_0}{B_m}\right)\varepsilon_0}$

microstructured matrix which comprises of a soft base polymeric matrix, PEGDA, in which a stiffer epoxy matrix (LY5052), further modified by MWCNTs, is embedded. At the next level, the microstructured matrices are considered as homogenized continuum materials in which polycrystalline $BaTiO_3$ piezoelectric inclusions are embedded. The properties of the polycrystal are derived from that of the single crystal. Therefore, considering the materials investigated here, Table 3 summarizes the electro-elastic properties of interest. The polymers (PEGDA and epoxy) studied in this investigation are elastically isotropic. i.e. their elastic coefficients are obtained from their isotropic Young's modulus E_m and Poisson's ratio ν_m, using the Lame's parameters given by $\lambda_m = \frac{E_m \nu_m}{(1+\nu_m)(1-2\nu_m)}$ and $\mu_m = \frac{E_m}{2(1+\nu_m)}$, as shown in Table 3. The Poisson's ratio for PEGDA is chosen to be equal to 0.35. Although

Table 3

Electroelastic properties of the constituent materials of the composites investigated in this study.

Material property	PEGDA [34–36]	Epoxy – LY5052 ([37] and datasheets)	Single crystal BaTiO₃ [3,38]
Elastic coefficients (Moduli in Pa)			
c_{11}	$\lambda_m + 2\mu_m$	$\lambda_m + 2\mu_m$	275.1×10^9
c_{13}	λ_m	λ_m	151.55×10^9
c_{33}	$\lambda_m + 2\mu_m$	$\lambda_m + 2\mu_m$	164.8×10^9
c_{44}	μ_m	μ_m	54.3×10^9
Young's modulus, E_m	1×10^6	1×10^9	–
Poisson's ratio, ν_m	0.35	0.35	–
Relative permittivity			
$\varepsilon_{11}/\varepsilon_0$	10	3.5	1970
$\varepsilon_{33}/\varepsilon_0$	10	3.5	109
Piezoelectric coefficients (Cm^{-2})			
e_{31}	0	0	−2.69
e_{33}	0	0	3.65
e_{15}	0	0	21.3

this is a rubber hydrogel, it is known that it is possible to reduce the Poisson's ratio from the rubbery limit (0.5) to smaller values through addition of solvents [34]. Hence, in fabricating these composite materials, the role of solvents is anticipated to be an important design criterion.

The embedded epoxy structures are further modified by addition of (15,15) MWCNTs. Addition of carbon nanotubes simultaneously stiffens the epoxy and increases its permittivity. We assume MWCNTs of aspect ratio ($AR = l/2r$) around 100, for which the percolation threshold is around $f_p = 0.7\%$ [39]. The critical exponent p is around 1 for CNT-modified polymer composites [40]. As mentioned in Section 2.1, we provide the effective properties of the embedded composite material as a function of the MWCNT concentration f_{CNT} in Appendix A1.

It is further known that the domain sizes in BaTiO₃ can be varied and sizes which are an order of magnitude smaller than the inclusion sizes considered here ($\approx 50 \mu$m) are possible to obtain [41], in addition to being amenable to tuning through material synthesis processes to obtain single crystals of sizes of the order of almost a millimeter [42]. This wide tunability in the crystallite sizes clearly shows that the polycrystallinity of the BaTiO₃ inclusions is a very important design parameter, the role of which, therefore, we will investigate here. The electro-elastic properties of polycrystalline BaTiO₃ are obtained from the properties of the single crystal as explained in [38] through the development of a self-consistent model for polycrystalline BaTiO₃. The effective properties of the polycrystal are expressed as a function of an orientation parameter α, such that the extremes $\alpha \to 0$ and $\alpha \to \infty$ correspond to fully oriented single crystal and randomly oriented polycrystal configurations, respectively. Intermediate values of α correspond to polycrystals with net grain-orientation along the direction of poling (which we assume to be along the x_3 direction here). The effective electro-elastic coefficients of polycrystalline BaTiO₃ are provided in Appendix A2. Here α is the standard deviation of the transversely isotropic Gaussian orientation distribution function that characterizes the statistical spread of the angles at which the c-axis of individual grains/domains in a polycrystal are oriented relative to the global direction of poling of the composite (i.e. the x_3 direction) [38].

3. Results and discussion

We discuss two design aspects in following two sections. In Section 3.1, we will first investigate the role of nanomodification in the auxetic embedded backbone of the matrix in tuning the mechanical coupling within the piezocomposite by controlling its auxeticity. Particularly, we will show that auxetic matrices can lead to a significant in the piezoelectric response to all the components of axial strain, therefore demonstrating the effectiveness of the design in high-performance energy harvesting composite materials. Following this, in Section 3.2, we will investigate the nonauxetic matrix structure. Particularly, we will demonstrate that the nonauxetic design, in conjunction with optimally polycrystalline inclusions, can lead to large anisotropies in the piezoelectric response of the composite. Through this we will demonstrate that the nonauxetic multiscale design is effective for designing anisotropic piezocomposites for directional sensing applications.

3.1. Isotropic improvement in piezoelectric response using nanomodified auxetic matrices

In this section, we consider a soft polymeric matrix (PEGDA) as a reference matrix material. This is further modified by embedding the nano-modified nonauxetic or auxetic network as shown in Fig. 1(b). As we mentioned earlier, the embedded microstructured network is modified at the nanoscale by uniform addition of MWCNTs. Considering the RVEs shown in Fig. 1(a)-(b), we obtain the effective elastic and dielectric properties of the nonauxetic and auxetic matrix architectures. The effective coefficients, for both the nonauxetic and auxetic architectures, are plotted in Fig. 3.

We note that the elastic coefficients of the matrices with the nanomodified embedded epoxy structures are around two orders of magnitude higher than the pristine PEGDA matrices, the elastic coefficients of which are the order of 10^6Pa (see Appendix A3). However, the effective coefficients in Fig. 3(a)-(d) are much lower compared to a matrix composed entirely of the nanomodified epoxy (see Appendix A1). Therefore, the microstructured matrix architecture, along with the nanomodification within the microstructure, allows achieving an intermediate matrix stiffness suitable for applications in flexible and wearable electronics [43,44]. Further, although both matrix architectures have a similar volume fraction of embedded material with similar CNT fill fractions, f_{CNT}, the auxetic matrix is relatively softer with smaller elastic moduli. The negative value of the effective c_{13} of the auxetic architecture confirms the auxetic effect. It is also clear that the auxetic effect becomes more pronounced at higher CNT concentrations. This is because as more CNTs are added to the embedded epoxy, it becomes relatively stiffer compared to the PEGDA matrix in which it is embedded, subsequently resulting in its predominance in determining the elastic properties of the composite matrix. Fig. 3(e)-(f) also show that the nanomodification within the embedded microstructures leads to a percolative and anisotropic increase in the permittivity of the multiscale matrices. Therefore, the multiscale design can lead to anisotropic tuning and improvement in both the elastic and the dielectric properties. We will next use these effective properties to evaluate the piezoelectric response of the composites possessing these matrix architectures.

Fig. 4 plots the effective piezoelectric response of the composites. Fig. 4(a)-(c), in sequence, show the effective coefficient e_{31}^{eff} of the composites based on the pristine PEGDA matrix, the nonauxetic and auxetic matrix architectures, respectively. For the composites with modified matrices, the effective coefficients are plotted as a function of both the inclusion volume fraction V_{BTO} and the CNT fill fraction, f_{CNT}, in the embedded structure. The composites with the pristine matrices show very weak piezoelectric response because of weak mechanical coupling of applied strains through the soft matrix, which absorbs most of the strain. However, both the modified matrices are stiffer than the pristine matrices and they also exhibit higher permittivities.

This firstly leads to improved coupling between the applied mechanical stimulus and the embedded piezoelectric inclusions.
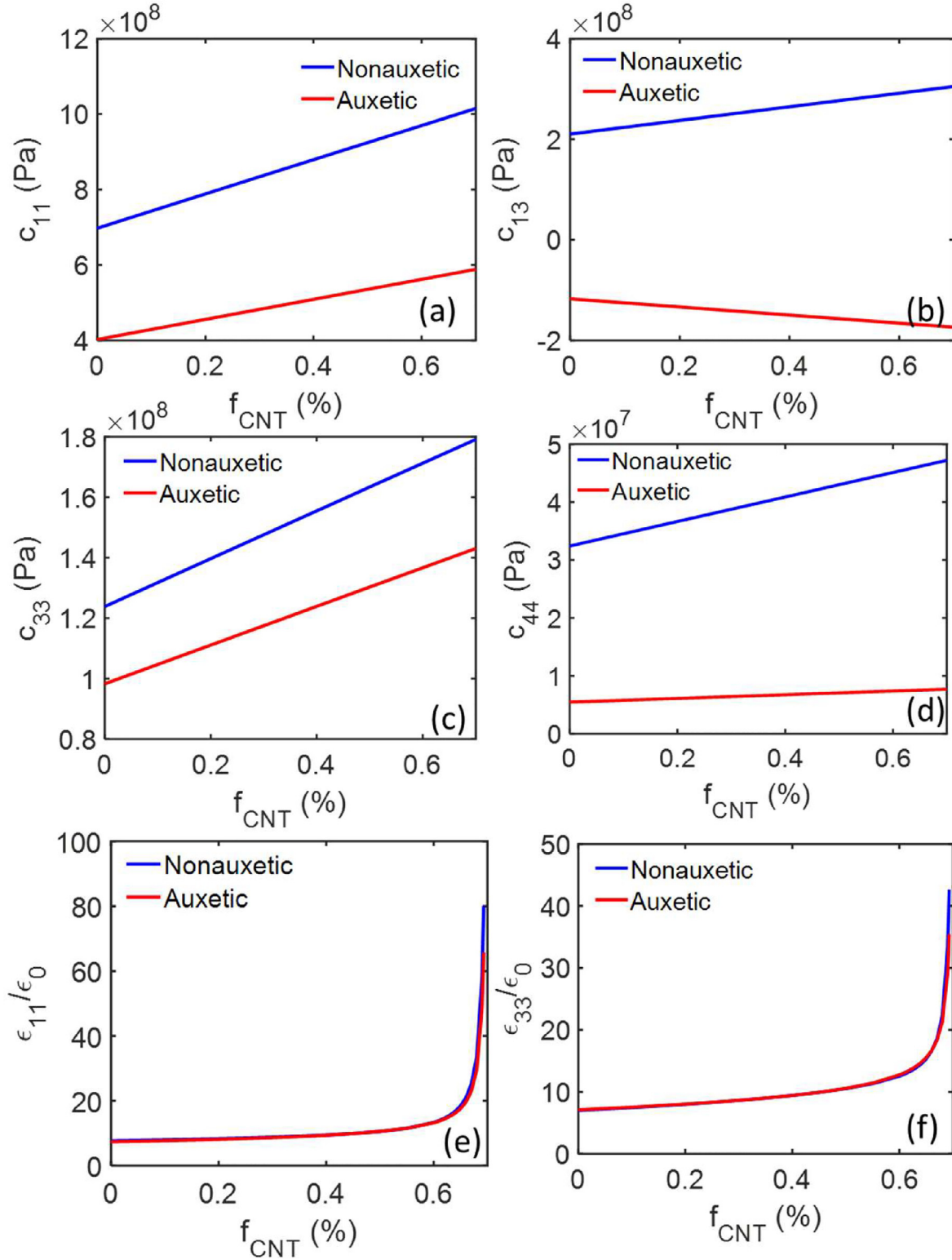
Fig. 3. The effective elastic ((a)-(d)) and dielectric (relative permittivity – (e)-(f)) properties of the nonauxetic and auxetic matrix designs shown in Fig. 1(b). These properties are used as bulk properties of a homogenized matrix material, in the next stage of computations relating to the piezoelectric composite behaviour.

Secondly, the improved permittivity also allows an easy passage to the electric flux generated within the inclusion. These factors together lead to around 2–3 orders of magnitude improvement in the piezoelectric response. On comparing the nonauxetic and auxetic architectures, we see from Fig. 4(b)-(c) that both designs lead to similar improvements in the effective coefficient e_{31}^{eff}. Further, on observing the effective coefficient e_{33}^{eff} in Fig. 4(e)-(f), we see that the auxetic matrix can lead to around an order of magnitude better improvement than the nonauxetic design. It is important to note that the permittivity of the auxetic matrix is slightly lesser that of the nonauxetic matrix, specially when the CNT volume fraction in the embedded epoxy structure, f_{CNT}, approaches the percolation threshold. Therefore, the observed
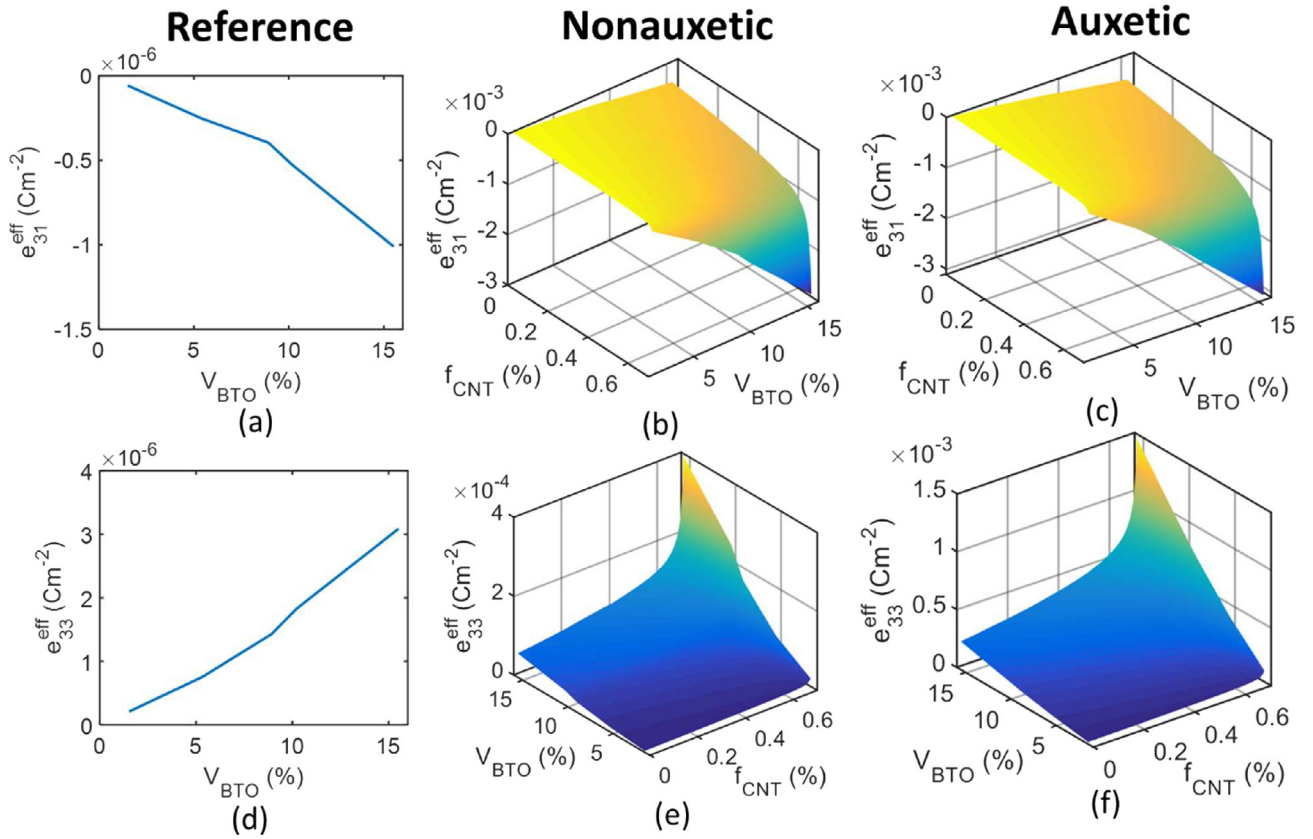
Fig. 4. The effective piezoelectric coefficients e_{31}^{eff} ((a)-(c)) and e_{33}^{eff} ((d)-(f)) of the composites based on the pristine PEGDA reference matrix ((a) and (d)), the nonauxetic ((b) and (d)) and auxetic multiscale matrix ((c) and (f)).

improvement in the auxetic design, over the nonauxetic one, is not due to better electrical characteristics of the matrix. This improvement is, therefore, clearly due to the enhanced mechanical coupling due to the auxetic effect. Also, in the case of the auxetic design, the improvements in e_{31}^{eff} and e_{33}^{eff} are comparable, therefore suggesting an isotropic improvement in piezoelectric response. This is particularly useful in the area of piezo-based energy harvesting, where directionality in response is not an important criterion and where designs yielding significantly high responses to all components of strain are desired. Therefore, the auxetic architecture leads to isotropic improvements in piezoelectric response, ideally suited for applications in energy harvesting.

Further, we observe from the effective elastic coefficients of the piezocomposites, shown in Fig. 5(a)-(c) for the nonauxetic design and Fig. 5(d)-(f) for the auxetic designs, that the auxetic design can give a softer composite while also leading to better a piezoelectric response compared to the nonauxetic design. The coefficient c_{13}^{eff} of the auxetic piezocomposite increases in magnitude on increasing either the nanotube or the inclusion volume fraction. This shows that there is a possibility to design composites with enhanced piezoelectric response having tunable auxeticity. In summary, we observe that the nanoengineered auxetic design can lead to significantly improved isotropic piezoelectric responses in addition to yielding soft composites suitable for application in flexible and wearable energy harvesting devices and circuits including important usage in the design and manufacturing sports and safety components [9,45,46].

Secondly, we also note that the nonauxetic multiscale design results in anisotropic improvements in e_{31}^{eff} and e_{33}^{eff}, with around an order of magnitude difference in the effective piezoelectric properties (Fig. 4 (b) and (e)). This can have interesting applications in the design of directional piezoelectric strain sensors. We will discuss this aspect of design in the next section.

3.2. Nanoengineered multiscale matrices with polycrystalline piezoelectric inclusions: Large anisotropies using nonauxetic matrices

In the previous section, we have demonstrated that auxetic matrices with nanoengineered microstructures can lead to better performing piezocomposites with reduced stiffening. Further, we also showed that the nonauxetic design can lead to anisotropic improvements in the piezoelectric response. This is an interesting observation in the context of directional sensing using piezoelectric devices. Obtaining directional strain sensing using piezoelectric materials is a challenge which requires materials with highly anisotropic piezoelectric responses [14,15]. Using the nonauxetic design, as shown here as an example can lead to an order of magnitude difference between the effective coefficients e_{31}^{eff} and e_{33}^{eff} and thus result in significant anisotropy in the strain sensing. Such materials can be used for directional strain sensing and can help bypass the requirement for additional sensors and circuitry that is required otherwise [14,15]. In this section, we will investigate the tunability in the piezoelectric anisotropy by using an optimal combination of multiscale matrix design and polycrystallinity of the inclusions.

For all the preceding analyses, we used single crystalline $BaTiO_3$ inclusions. In this section, we will investigate the effect of using a multiscale matrix on the behaviour of polycrystalline $BaTiO_3$ inclusions. The polycrystalline state of the inclusion affects all its electro-elastic properties [38] and it is expected that the anistropic elastic and electrical properties of the engineered matrices will interact with these polycrystalline effects resulting in possible design insights and optimizations. As we mentioned earlier, the electroelastic properties of polycrystalline $BaTiO_3$ are modelled based on orientational averaging, starting from the properties of the single crystal which are given in Table 3. For this analysis, we assume that the nanotubes within the
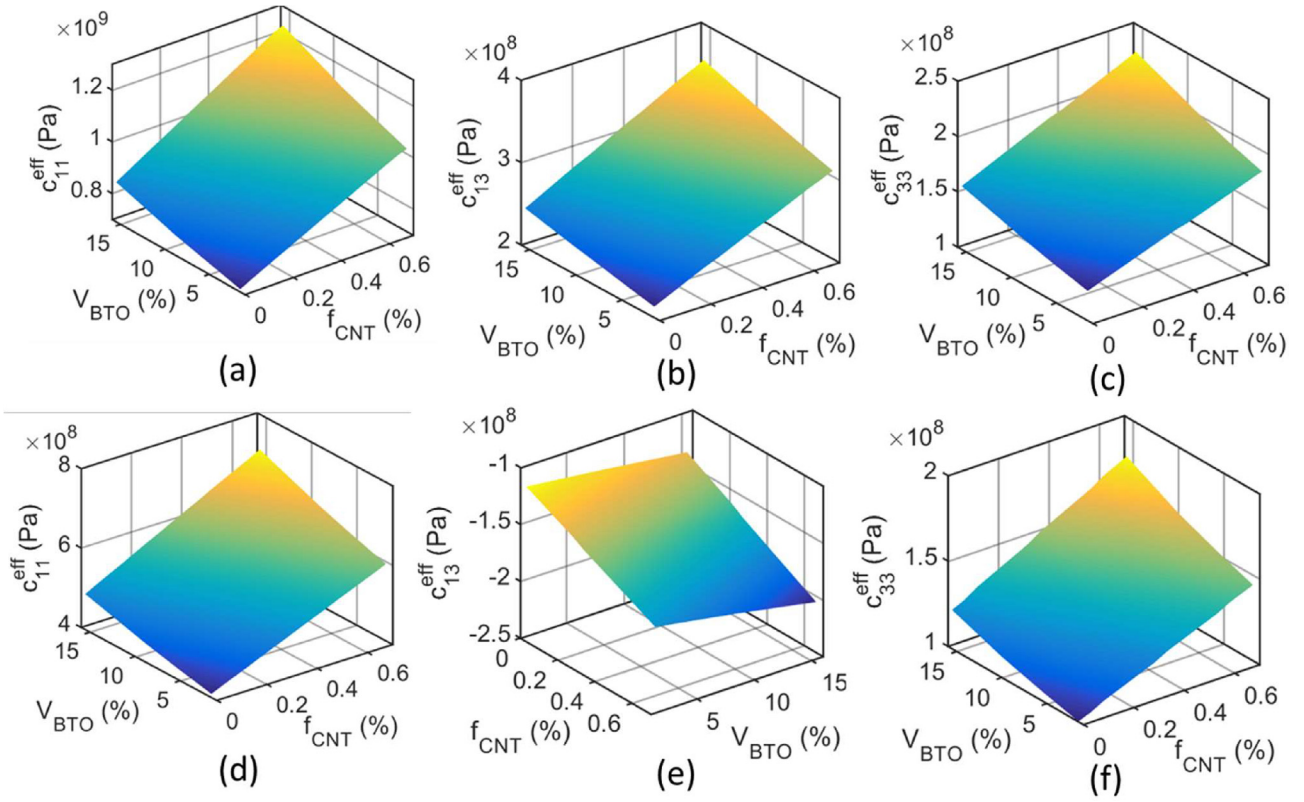
Fig. 5. The effective elastic coefficients of piezocomposites based on the (a)-(c) nonauxetic and (d)-(f) auxetic multiscale matrices.

embedded epoxy microstructures in the engineered matrices are near percolation, i.e. we assume $f_{CNT} = 0.99f_p$.

Fig. 6 (a)-(c) show the effective elastic coefficients of the piezocomposite based on the reference pristine PEGDA matrix, the nonauxetic and auxetic engineered matrices, as a function of the polycrystalline index α. It is seen that the elastic coefficients are almost independent of the polycrystalline state of the inclusions. Irrespective of the polycrystallinity of the inclusion, the engineered matrices show elastic moduli which are 2–3 magnitudes higher than the pristine soft matrix and also that the auxetic matrix is relatively softer than the nonauxetic matrix, by virtue of its geometry alone. Fig. 6(d)-(e) show that effective piezoelectric coefficients of the composite are strongly dependent on α. We still see that single crystals ($\alpha \rightarrow 0$) still show the best performance. There is an enhancement of 3 orders of magnitude in the effective coefficient e_{31}^{eff}. We observe that both the engineered matrices have similar effects here. However, in the case of the effective coefficient e_{33}^{eff}, the auxetic design leads to a much better improvement. This is what we also saw in the previous section. To understand the difference between the two engineered matrices, we plot the relative differences between the piezoelectric coefficients between the two matrices in Fig. 6(f), given by

$$\Delta e_{31} = \frac{e_{31}^{eff,a} - e_{31}^{eff,n}}{e_{31}^{eff,n}}, \Delta e_{33} = \frac{e_{33}^{eff,a} - e_{33}^{eff,n}}{e_{33}^{eff,n}} \quad (3)$$

where the a and the n in the superscripts refer to the auxetic and nonauxetic matrices, respectively. We see two different trends for the coefficients e_{31}^{eff} and e_{33}^{eff}. First, in the case of e_{31}^{eff}, the auxetic composite is only slightly better than the nonauxetic matrices, specially in the composites with single-crystal-like inclusions (small α). However, in the case of e_{33}^{eff}, the auxetic design has a pronounced enhancement in the piezoelectric response for larger α(polycrystals), where its performance can be at least 12 times better than the nonauxetic design. This

shows that using auxetic matrices can lead to distinct advantages in the case of polycrystalline inclusions. In practical terms, this means that single crystalline inclusions may not always be desirable and the set back in the performance, on using polycrystal inclusions, could be compensated by using nanoengineered auxetic matrices.

A further important aspect of design, specifically in the area sensors, is that of directional detection, as highlighted in Section 3.1. It is important to have piezocomposites which can have a large contrast in their sensitivity to different strain components. We anticipated that introducing anisotropic microstructures into the matrix can help design such anisotropic piezocomposites and we demonstrated this with single crystal inclusions in Section 3.1. Here, we further analyze the role of the polycrystallinity of the inclusions in tuning the anisotropy. We define the anisotropy $A(\alpha)$ in terms of the ratio of the sensitivity of the composite to transverse (ε_{11}) and longitudinal (ε_{33}) strains, given by the ratio of the respective piezoelectric coefficients as

$$A(\alpha) = \left| \frac{e_{31}^{eff}(\alpha)}{e_{33}^{eff}(\alpha)} \right| \quad (4)$$

We plot this quantity as a function of α, for composites based on both engineered matrices, in Fig. 7. In this case, the auxetic design results in an anisotropy around 2, which is almost independent of α. However, the nonauxetic design, based on the hexagonal unit cell, shows much larger anisotropies with a strong dependence on α. For larger value of α,or synonymously, in composites with relatively wider polycrystalline orientation distributions, the nonauxetic engineered matrix design can exhibit anisotropies exceeding 30. Fig. 6(d)-(e) suggests that this increase in anisotropic piezoelectric response is also inevitably accompanied by a reduction in the overall piezoelectric sensitivity. However, the piezoelectric coefficients of the engineered composites are still significantly larger than the reference composite design, and an optimal polycrystalline configuration can be chosen in conjunction with the nonauxetic nanoengineered matrix design to
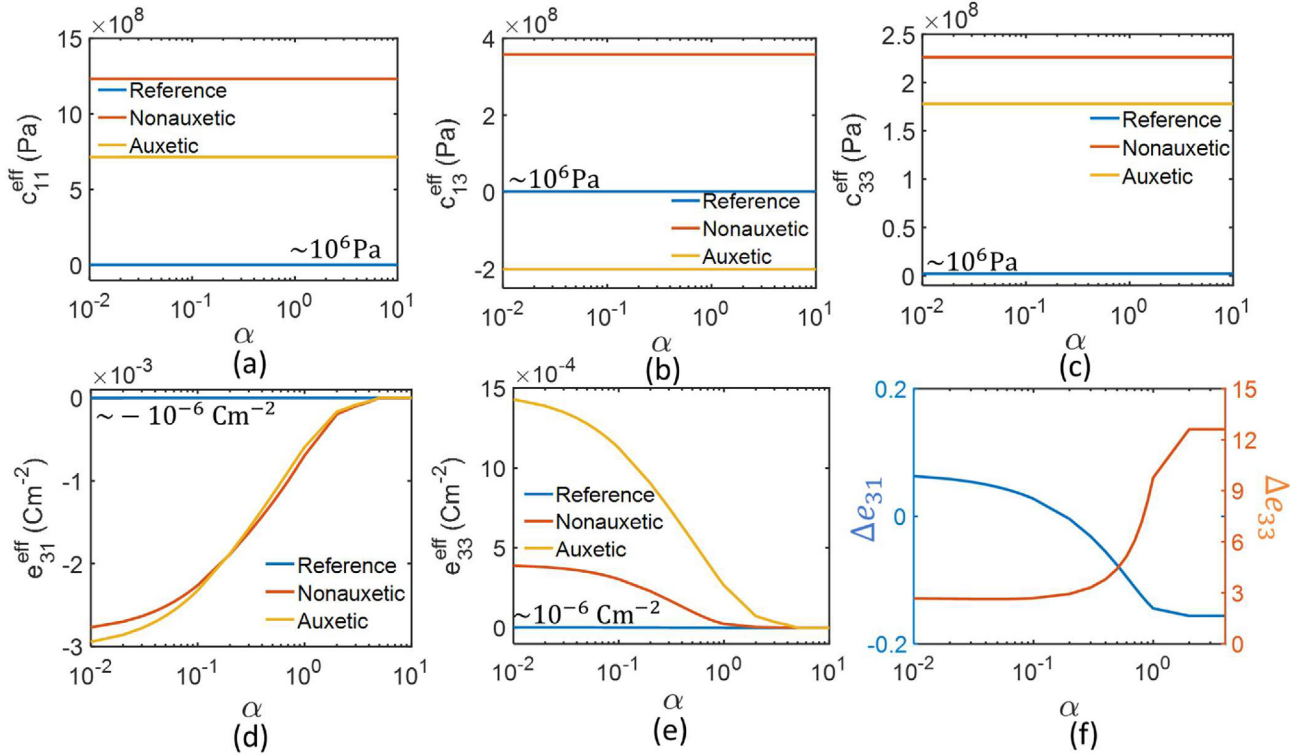
Fig. 6. (a)-(c) The effective elastic moduli, and (d)-(e) the effective piezoelectric coefficients of piezocomposites based on the reference PEGDA matrix and the engineered nonauxetic and auxetic matrices, respectively, (f) shows the relative difference between the piezoelectric coefficients of the auxetic and nonauxetic designs.
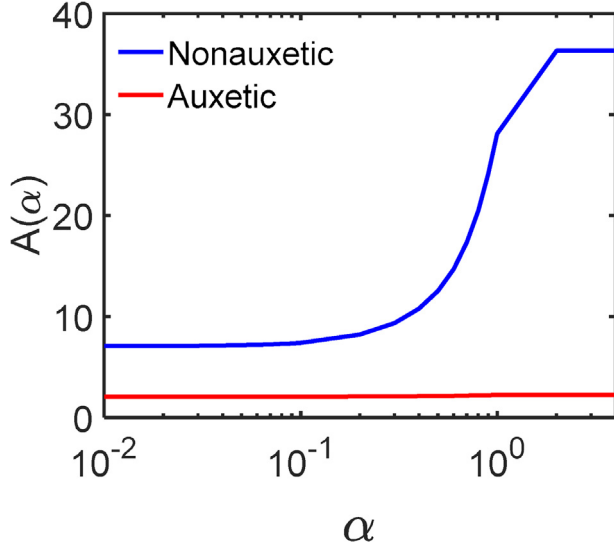

Fig. 7. The anisotropy $A(\alpha) = \left| \dfrac{e_{31}^{eff}(\alpha)}{e_{33}^{eff}(\alpha)} \right|$ in the piezoelectric response of the engineered piezoelectric designs.

make piezoelectric materials with sufficiently large anisotropies. This has very important implications for applications in directional sensing. This is because current sensor technologies based on piezoelectric ceramics are limited by the transverse anisotropy of the piezoelectric material which does not allow unique measurements of all components of strain [14,15]. The approach demonstrated here (and similar approaches developed based on the idea of anisotropic composite design through geometric tuning of the matrix architecture) can help overcome these pressing challenges of sensor design.

Finally, we note that both the auxetic and nonauxetic nanoengineered matrices are useful in different ways. The auxetic matrix can lead to better mechanical coupling and thus a considerable improvement in the piezoelectric response, with similar improvements in sensitivity to transverse and longitudinal strains. The nonauxetic matrix is important in the context of sensing technology due to the possibility of designing highly anisotropic piezocomposites by combining matrix microstructures, nanoadditions, and inclusion polycrystallinity.

4. Summary

We have demonstrated a new design route to engineer the performance and directional sensitivity of lead-free piezoelectric composites. The idea was based on using a multiscale design for the matrix component, which involved a base matrix material in which anisotropic microstructured networks of relatively stiffer polymers are embedded. Further, these networks are also subject to nanomodification of their elastic and electrical properties through addition of carbon nanotubes. We studied two microstructured networks – a nonauxetic network with repeating hexagonal cells and an auxetic network with repeating inverted hexagonal cells. The piezoelectric inclusions are polycrystalline lead-free materials. Our simulations highlight two key results.

(a) The auxetic matrices lead to improved coupling between the applied mechanical stimuli and the inclusions, resulting in amplified strains within the inclusions. This leads to composites with significantly better piezoresponses which are 2–3 orders of magnitude better than the reference design. The auxetic design is also an order of magnitude better than the nonauxetic design in sensing out-of-plane (ε_{33}) strains. Further, the auxeticity and the associated improvements in piezoelectric response, can be tuned by nanomodification within the auxetic embedded polymeric structures with larger CNT concentrations leading to both
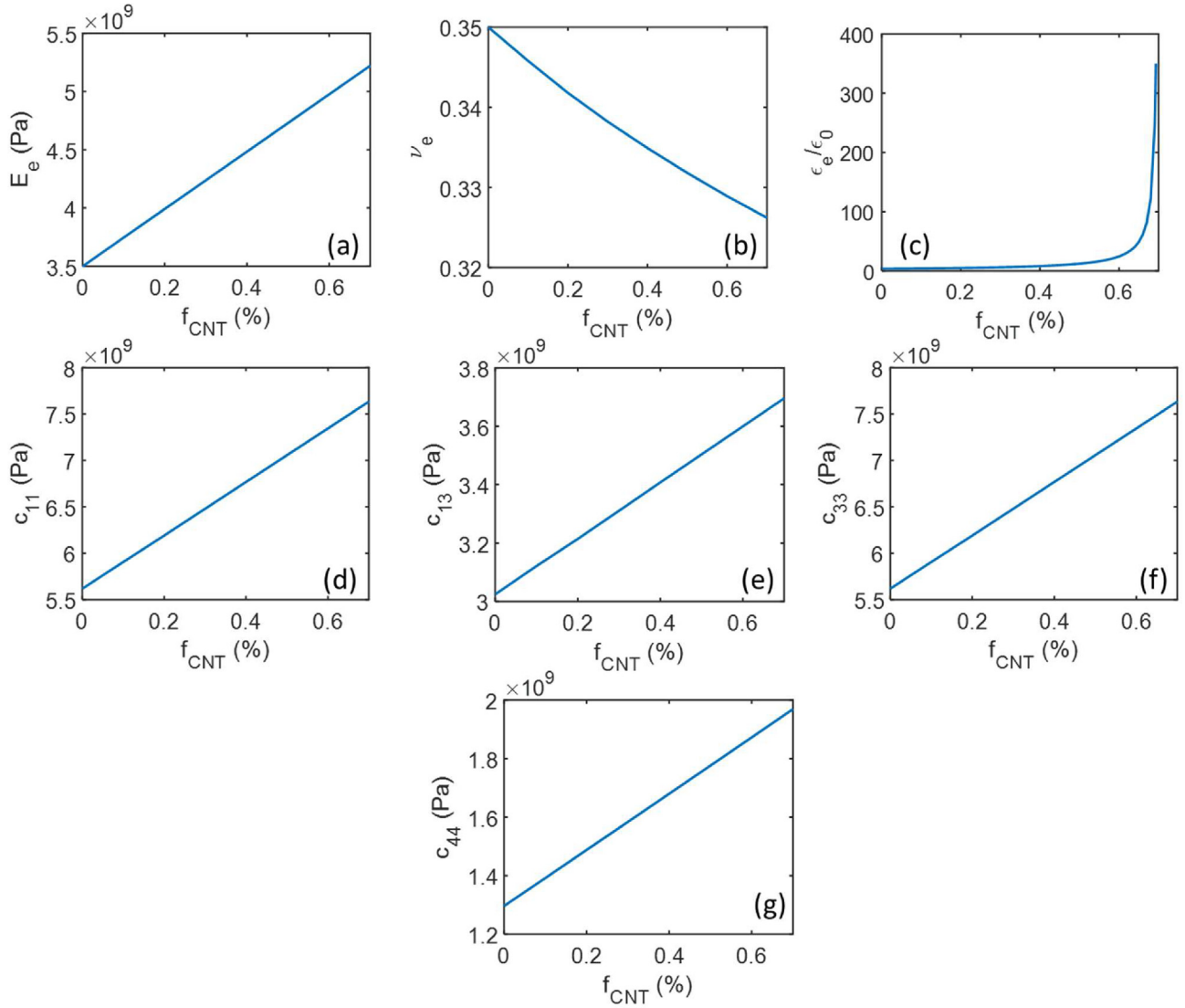
Fig. AF1. Effective electro-elastic coefficient of CNT-modified epoxy, used as the material constituting the stiff microstructures embedded in soft polymeric matrices shown in Fig. 1(b). (a) and (b) are the effective Young's modulus and the Poisson's ratio, respectively, (c) is the effective relative permittivity, (d)-(g) are the effective elastic coefficients calculated from (a)-(b).
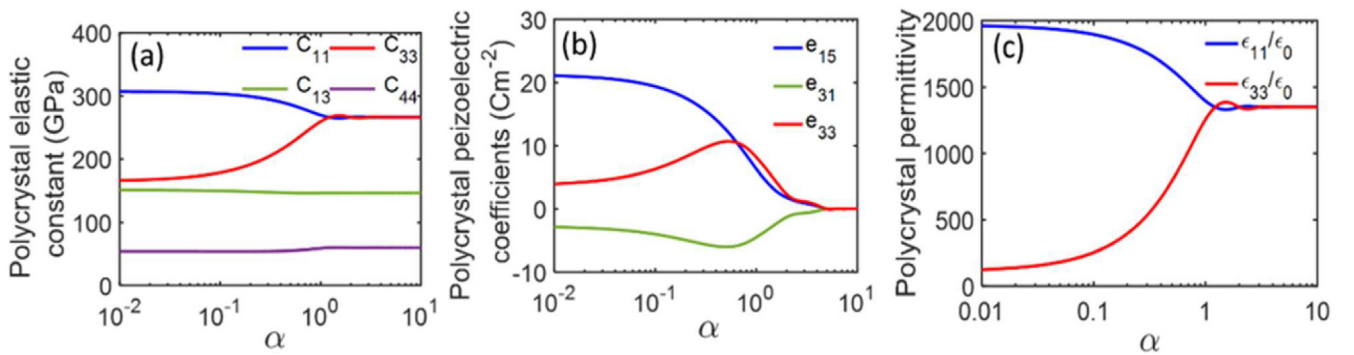

Fig. AF2. The effective electro-elastic coefficients of polycrystalline BaTiO$_3$.

better strain-coupling and higher overall matrix permittivities, which underlie the significant boosts in the piezoelectric response. Although the geometry of the auxetic structure is anisotropic, the overall design shows similar improvements in the sensitivity to all the components of axial strains. Also, this improvement comes with a relatively soft matrix because the design, in principle, decouples matrix stiffness and strain-coupling to inclusions. This shows that this design could be very

Table AT1
The effective elastic coefficients of PEGDA.

Elastic coefficient	Value (Pa)
c_{11}	1.6×10^6
c_{13}	8.64×10^5
c_{33}	1.6×10^6
c_{44}	3.7×10^5

interesting in energy harvesting applications with some niche areas of interest being the design of energy harvesting conformable and wearable sports equipment.

(b) The nonauxetic matrices show a large contrast in their response to the in-plane and out-of- plane strains (ε_{11} and ε_{33}, respectively). A proper choice of polycrystalline inclusions in conjunction with the nonauxetic nanoengineered matrix can help design piezocomposites with large anisotropies. This has important implications in sensor technology where anisotropic materials which have directional sensitivity are critical.

Overall, we have demonstrated that nanoengineered multiscale design of matrices with nonauxetic or auxetic microstructures, coupled with polycrystalline piezoelectric inclusions, can be a very compelling route to tune the performance of piezocomposites to suit the widely different needs of applications such as energy harvesting and sensing.

Declaration of Competing Interest

The authors declare that they have no known competing financial interests or personal relationships that could have appeared to influence the work reported in this paper.

Acknowledgements

Appendix

A1: The effective elastic and dielectric properties of CNT-modified epoxy

The stiff polymeric structures embedded in the soft PEGDA matrices, to design composite matrices, are made of epoxy LY5052 modified by the addition of (15,15) MWCNTs. The effective elastic properties are obtained through a micromechanics approach highlighted in [29]. Further, the permittivity of the CNT-modified epoxy follows a percolative behaviour given by

$$\varepsilon^{eff} = \varepsilon \left(\frac{f_p}{f_p - f_{CNT}} \right)^p \tag{AE1}$$

where ε is the relative permittivity of the pristine epoxy, f_{CNT} is the concentration of the nanotubes in the epoxy matrix, f_p is the percolation threshold of CNTs in epoxy, and p is the critical exponent related to the percolation. As explained in section 3.3, we have $f_p = 0.7\%$ and $p = 1.0$. The effective elastic properties obtained from the above approaches are plotted in Fig. AF1.

In Fig. AF1, E_e and ν_e are the Young's modulus and the Poisson's ratio of the composite material, respectively. The composite is isotropic and hence its elastic properties are calculated using the following Lame's parameters

$$\lambda_e = \frac{E_e \nu_e}{(1 + \nu_e)(1 - 2\nu_e)}, \mu_e = \frac{E_e}{2(1 + \nu_e)} \tag{A2}$$

The elastic coefficients are calculated as

$$c_{11} = c_{33} = \lambda_e + 2\mu_e, c_{13} = \lambda_e, c_{44} = \mu_e \tag{A3}$$

A2: The effective electro-elastic coefficients of polycrystalline BaTiO$_3$

The polycrystallinity of BaTiO$_3$ inclusions is quantitatively represented through the parameter α, the interpretation of which has been provided in section 2.3. The effective coefficients – elastic, dielectric, and piezoelectric – of the polycrystals as a function of α are shown in Fig. AF2.

A3: The elastic properties of the base PEGDA matrix

PEGDA forms the soft base matrix in which the epoxy structures are embedded, as shown in Fig. 1(b). It is an isotropic material and hence the elastic coefficients of PEGDA are calculated following equations AE2-AE3. These properties are listed in Table AT1. These coefficients are calculated by assuming the following values for the elastic properties of the matrix, following the entries in Table 3: $E = 1$MPa and $\nu = 0.35$. The elastic coefficients of the PEGDA matrix are 3–4 orders of magnitude smaller than those of the CNT-modified epoxy (Table AT1.).

References

[1] Maurya D, Peddigari M, Kang M-G, Geng LD, Sharpes N, Annapureddy V, Palneedi H, Sriramdas R, Yan Y, Song H-C, Wang YU, Ryu J, Priya S. Lead-free piezoelectric materials and composites for high power density energy harvesting. J Mater Res 2018;33(16):2235–63.

[2] Kim H, Torres F, Islam MT, Islam MD, Chavez LA, Garcia Rosales CA, Wilburn BR, Stewart CM, Noveron JC, Tseng T-L, Lin Y. Increased piezoelectric response in functional nanocomposites through multiwall carbon nanotube interface and fused-deposition modeling three-dimensional printing. MRC 2017;7(4):960–6.

[3] Berlincourt D, Jaffe H. Elastic and piezoelectric coefficients of single-crystal barium titanate. Phys Rev 1958;111(1):143–8.

[4] Odegard GM. Constitutive modeling of piezoelectric polymer composites. Acta Mater 2004;52(18):5315–30.

[5] Johnston ID, McCluskey DK, Tan CKL, Tracey MC. Mechanical characterization of bulk Sylgard 184 for microfluidics and microengineering. J Micromech Microeng 2014;24(3):035017. https://doi.org/10.1088/0960-1317/24/3/035017.

[6] Rafiee MA, Rafiee J, Yu Z-Z, Koratkar N. Buckling resistant graphene nanocomposites. Appl Phys Lett 2009;95(22):223103. https://doi.org/10.1063/1.3269637.

[7] Rafiee MA, Rafiee J, Srivastava I, Wang Z, Song H, Yu Z-Z, Koratkar N. Fracture and fatigue in graphene nanocomposites. Small 2010;6(2):179–83.

[8] Rafiee MA, Rafiee J, Wang Z, Song H, Yu Z-Z, Koratkar N. Enhanced mechanical properties of nanocomposites at low graphene content. ACS Nano 2009;3 (12):3884–90.

[9] Sanami M, Ravirala N, Alderson K, Alderson A. Auxetic materials for sports applications. Proc Eng 2014;72:453–8.

[10] Shi K, Sun B, Huang X, Jiang P. Synergistic effect of graphene nanosheet and BaTiO3 nanoparticles on performance enhancement of electrospun PVDF nanofiber mat for flexible piezoelectric nanogenerators. Nano Energy 2018;52:153–62.

[11] Huang L, Lu C, Wang F, Wang Lu. Preparation of PVDF/graphene ferroelectric composite films by in situ reduction with hydrobromic acids and their properties. RSC Adv 2014;4(85):45220–9.

[12] Kim GH, Hong SM, Seo Y. Piezoelectric properties of poly(vinylidene fluoride) and carbon nanotube blends: β-phase development. Phys Chem Chem Phys 2009;11 (44):10506. https://doi.org/10.1039/b912801h.

[13] Lee JS, Kim GH, Kim WN, Oh KH, Kim HT, Hwang SS, Hong SM. Crystal structure and ferroelectric properties of poly(vinylidene fluoride)-carbon nano tube nanocomposite film. Mol Cryst Liq Cryst 2008;491(1):247–54.

[14] Cui H, Hensleigh R, Yao D, Maurya D, Kumar P, Kang MG, Priya S, Zheng X. Three-dimensional printing of piezoelectric materials with designed anisotropy and directional response. Nature Mater 2019;18(3):234–41.

[15] Sirohi J, Chopra I. Fundamental understanding of piezoelectric strain sensors. J Intell Mater Syst Struct 2000;11(4):246–57.

[16] Kim K, Zhu W, Qu X, Aaronson C, McCall WR, Chen S, Sirbuly DJ. 3D optical printing of piezoelectric nanoparticle–polymer composite materials. ACS Nano 2014;8(10):9799–806.

[17] Phatharapeetranun N, Ksapabutr B, Marani D, Bowen JR, Esposito V. 3D-printed barium titanate/poly-(vinylidene fluoride) nano-hybrids with anisotropic dielectric properties. J Mater Chem C 2017;5(47):12430–40.

[18] Krishnaswamy JA, Buroni FC, Melnik R, Rodriguez-Tembleque L, Saez A. Design of polymeric auxetic matrices for improved mechanical coupling in lead-free piezocomposites. Smart Mater Struct 2020;29(5):054002. https://doi.org/10.1088/1361-665X/ab7e35.

[19] Lakes RS. Negative-Poisson's-ratio materials: auxetic solids. Annu Rev Mater Res 2017;47(1):63–81.

[20] Li Q, Kuang Y, Zhu M. Auxetic piezoelectric energy harvesters for increased electric power output. AIP Adv 2017;7(1):015104. https://doi.org/10.1063/1.4974310.

[21] Topolov VY, Bowen CR. High-performance 1–3-type lead-free piezo-composites with auxetic polyethylene matrices. Mater Lett 2015;142:265–8.

[22] Lakes R. Materials with structural hierarchy. Nature 1993;361(6412):511–5.

[23] Shufrin I, Pasternak E, Dyskin AV. Hybrid materials with negative Poisson's ratio inclusions. Int J Eng Sci 2015;89:100–20.

[24] Ramírez M, Nava-Gómez GG, Sabina FJ, Camacho-Montes H, Guinovart-Díaz R, Rodríguez-Ramos R, Bravo-Castillero J. Enhancement of Young's moduli and auxetic windows in laminates with isotropic constituents. Int J Eng Sci 2012;58:95–114.

[25] Pasternak E, Dyskin AV. Materials and structures with macroscopic negative Poisson's ratio. Int J Eng Sci 2012;52:103–14.

[26] Agnelli F, Constantinescu A, Nika G. Design and testing of 3D-printed micro-architectured polymer materials exhibiting a negative Poisson's ratio. Continuum Mech Thermodyn 2020;32(2):433–49.

[27] Li J, Ma PC, Chow WS, To CK, Tang BZ, Kim J-K. Correlations between percolation threshold, dispersion state, and aspect ratio of carbon nanotubes. Adv Funct Mater 2007;17(16):3207–15.

[28] Wang F, Wang J-W, Li S-Q, Xiao J. Dielectric properties of epoxy composites with modified multiwalled carbon nanotubes. Polym Bull 2009;63(1):101–10.

[29] Rodríguez-Tembleque L, García-Macías E, Sáez A. CNT-polymer nanocomposites under frictional contact conditions. Compos B Eng 2018;154:114–27.

[30] Qin R-S, Xiao Yi, Lan H. Numerical simulation of effective properties of 3D piezoelectric composites. J Eng 2014;2014:1–14.

[31] Saputra AA, Sladek V, Sladek J, Song C. Micromechanics determination of effective material coefficients of cement-based piezoelectric ceramic composites. J Intell Mater Syst Struct 2018;29(5):845–62.

[32] Sladek J, Sladek V, Krahulec S, Song C. Micromechanics determination of effective properties of voided magnetoelectroelastic materials. Comput Mater Sci 2016;116:103–12.

[33] Piefort V 2001 Finite element modelling of piezoelectric active structures. Ph. D. thesis. Bruxelles, Belgium: Université Libre de Bruxelles, Department …)

[34] Cappello J, d'Herbemont V, Lindner A and du Roure O 2020 Microfluidic In-Situ Measurement of Poisson's Ratio of Hydrogels Micromachines 11 318

[35] Turturro M V, Sokic S, Larson J C and Papavasiliou G 2013 Effective tuning of ligand incorporation and mechanical properties in visible light photopolymerized poly (ethylene glycol) diacrylate hydrogels dictates cell adhesion and proliferation Biomedical Materials 8 025001

[36] Popielarz R, Chiang CK, Nozaki R, Obrzut J. Dielectric properties of polymer/ferroelectric ceramic composites from 100 Hz to 10 GHz. Macromolecules 2001;34(17):5910–5.

[37] Raponi O d A, Raponi R d A, Barban G B, Benedetto R M D and Ancelotti Junior A C 2017 Development of a Simple Dielectric Analysis Module for Online Cure Monitoring of a Commercial Epoxy Resin Formulation Materials Research 20 291-7

[38] Li JY. The effective electroelastic moduli of textured piezoelectric polycrystalline aggregates. J Mech Phys Solids 2000;48(3):529–52.

[39] Bao H-D, Sun Y, Xiong Z-Y, Guo Z-X, Yu J. Effects of the dispersion state and aspect ratio of carbon nanotubes on their electrical percolation threshold in a polymer. J Appl Polym Sci 2013;128(1):735–40.

[40] Li Q, Xue Q, Hao L, Gao X, Zheng Q. Large dielectric constant of the chemically functionalized carbon nanotube/polymer composites. Compos Sci Technol 2008;68(10-11):2290–6.

[41] Wada S, Yako K, Kakemoto H, Tsurumi T, Kiguchi T. Enhanced piezoelectric properties of barium titanate single crystals with different engineered-domain sizes. J Appl Phys 2005;98(1):014109. https://doi.org/10.1063/1.1957130.

[42] Hulm JK. Dielectric properties of single crystals of barium titanate. Nature 1947;160(4056):127–8.

[43] Hwang G-T, Byun M, Jeong CK, Lee KJ. Flexible piezoelectric thin-film energy harvesters and nanosensors for biomedical applications. Adv Healthcare Mater 2015;4(5):646–58.

[44] Lee M, Chen C-Y, Wang S, Cha SN, Park YJ, Kim JM, Chou L-J, Wang ZL. A hybrid piezoelectric structure for wearable nanogenerators. Adv Mater 2012;24(13):1759–64.

[45] Allen T, Martinello N, Zampieri D, Hewage T, Senior T, Foster L, Alderson A. Auxetic foams for sport safety applications. Procedia Eng 2015;112:104–9.

[46] Duncan O, Foster L, Senior T, Allen T, Alderson A. A comparison of novel and conventional fabrication methods for auxetic foams for sports safety applications. Procedia Eng 2016;147:384–9.